https://doi.org/10.1016/j.jallcom.2015.11.100

Saw-tooth-like bulk metallic glass structures with greatly enhanced energy-absorption performance

S.H. Chen[1], K.C. Chan[1]*, G. Wang[1,2] and J. Yi[1]

[1]Advanced Manufacturing Technology Research Centre, Department of Industrial and Systems Engineering, The Hong Kong Polytechnic University, Hung Hom, Kowloon, Hong Kong.

[2]Laboratory for Microstructures, Shanghai University, Shanghai 200444, China

* Corresponding author. Tel.: +852 27664981. E-mail address: kc.chan@polyu.edu.hk (K.C. Chan).

Abstract

In this work, saw-tooth-like bulk metallic glass (BMG) structures were developed, exhibiting greatly enhanced energy-absorption performance as compared with existing cellular metals, such as conventional metal foams and BMG foams/honeycombs. The excellent energy absorption capacity is attributed to the change of the deformation modes from bending, buckling and collapse of the structural units in conventional cellular solids to large plastic deformation in the present BMG structures. Additionally, the energy absorption capacity of designed saw-tooth-like BMG structures can also be tuned by tailoring the periodic distribution of the structural units.

Key words: Cellular materials; Energy absorption capacity; Bulk metallic glass; Shear bands.

1. Introduction

Cellular solids with high energy absorption capacity have wide applications for crash protection and blast mitigation, such as in automotive industries, light-weight constructions and supporting cores of structural sandwich panels [1-6]. Due to the large energy absorption capacity by forming a steady plastic-flow stage, cellular metals have been studied extensively for energy-absorption purpose [7,8]. For example, Al and Al alloy foams have demonstrated a wide range of porosity, a high specific strength and a high energy absorption capacity [1,9]. Research findings have demonstrated that the energy-absorption performance of cellular materials is significantly influenced by the strength of the parent materials [7]. By replacing the parent Al alloys using metals with relatively-higher strength, some other alloy based foams have then been developed, such as steel foams [10], copper foams [11] and composite metal foams [12,13], exhibiting better energy-absorption performance.

As a novel class of structural materials, bulk metallic glasses (BMGs) are known to have relatively higher hardness and strength than their crystalline counterparts [14-16]. This enables BMGs to become ideal parent materials to fabricate cellular structures for energy-absorption applications. Some BMG structures, such as BMG foams [17-20] and honeycombs [21,22], have been developed and have demonstrated better energy-absorption performance than conventional Al foams. However, when compared with other alloy foams [10-13], the energy-absorption performance of these BMG structures shows no obvious advantages. Some recent work has shown that to

increase the plastic deformation in the structural units could further improve the energy-absorption performance of BMG structures [23,24]. BMGs are able to demonstrate more plastic deformation behavior under complex stress states than uniform stress states [25-28]. In fact, in practical applications of structural materials, the material always deforms under complex stress states, rather than uniform compressive or tensile stresses [29-31]. In this work, by the use of the large plastic deformation behavior of BMGs under complex stress states, some saw-tooth-like BMG structures have been designed and fabricated, where the deformation modes are mainly plastic deformation under compressive testing. These BMG structures have demonstrated much enhanced energy absorption capacity than previously reported metal foams and BMG structures.

2. Experimental

The design of a single tooth unit of saw-tooth-like BMG structures is shown in the schematic diagram in Fig. 1. The saw-tooth-like BMG structure consists of a substrate and periodically distributed tooth units. The distances between the symmetric planes of the tooth units (d_3 in Fig. 1) were tailored as 2.8 mm, 2.2 mm and 1.6 mm for specimens A, B and C, respectively. To fabricate the saw-tooth-like BMG structures, as-cast $Zr_{57}Cu_{20}Al_{10}Ni_8Ti_5$ (at.%) BMG rods of 5 mm diameter were prepared by suction-casting the melted ingots in a copper mold, from the pure elements of Zr, Cu, Al, Ni, and Ti. The amorphous atomic structure of the as-cast BMG specimens was confirmed using standard X-ray diffraction (XRD) analysis on a Rigaku SmartLab

X-ray diffractometer. The saw-tooth-like structures were then fabricated from the as-cast rods using wire-cut electrical discharge machining (EDM) on an FI 240 SLP wire-cut EDM machine. After EDM, the side surfaces of the specimens were polished using abrasive paper with grit sizes from 150 to 2000. The relative densities of the saw-tooth-like BMG structures were calculated using the equation

$$\rho_{\mathrm{r}} = \frac{\rho_{\mathrm{s}}}{\rho_{\mathrm{p}}} = \frac{n\frac{(d_1 + d_2)}{2}h_1 + (n-1)d_3 + d_2}{[(n-1)d_3 + d_2]\mathrm{of}(h_1 + h_2)} \qquad (1)$$

where ρ_{s} and ρ_{p} are the densities of the saw-tooth-like BMG structures and the parent BMGs respectively, and n is the number of the tooth unit. The relative densities of specimens A (n = 5), B (n = 6) and C (n = 8) were calculated as 0.52, 0.56 and 0.62, respectively. Three saw-tooth-like structures with relative densities of 0.52, 0.56 and 0.62 respectively made of a high-strength stainless steel (SS316L) have also been prepared to make a comparison. Compression tests of the saw-tooth-like BMG structures were conducted on a servo-hydraulic 810 Materials Testing System (MTS) at a constant cross-head loading speed of 0.036 mm/min. After compressive testing, the side surfaces of the deformed specimens were examined using scanning electron microscopy (SEM) on a Jeol JSM-6490 scanning electron microscope.

3. Results and discussion

The compressive deformation behavior of the saw-tooth-like BMG structures is shown in Fig. 2a. Although BMGs are known to have a size effect [32,33], and the

bulk form of a $Zr_{57}Cu_{20}Al_{10}Ni_8Ti_5$ BMG specimen of 5 mm diameter has very limited macroscopic strain (about 1% plastic strain) [23], the saw-tooth-like BMG structures have wide plastic-flow plateau stages till densification. Moreover, besides the slight decrease of the nominal stresses before the densification stage in specimens A and C, all the specimens have continuously increasing nominal stresses during the plastic-flow plateau stages. The stress decay factors f_d of the saw-tooth-like BMG structures were estimated using the expression [24]

$$f_d = (\sigma_{onset} - \sigma_d)/(\varepsilon_d - \varepsilon_{onset}) \qquad (2)$$

where σ_{onset} and ε_{onset} are the nominal stress and macroscopic strain at the onset of the plastic-flow stage, and σ_d and ε_d are the values at densification. The calculated f_d values for specimens A-C are -10.6 MPa/1%, -15.8 MPa/1% and -22.5 MPa/1%, respectively. When compared with the decay of the peak stresses during the plastic-flow plateau stages in the cellular BMGs with macroscopic cellular structures [24], the present saw-tooth-like BMG structures have high rates of increase in the nominal stresses. Since BMGs are known to have work-softening behavior, the increase of nominal stresses should result from the specially-designed trapezoidal structural units. It has been reported that, under compression tests, BMG specimens with sizes less than 1 mm have large macroscopic strains [32,33]. The resultant stress gradient stemming from the trapezoidal shape under compression not only increases the plastic deformation but also achieves work-hardening-like behavior, leading to large macroscopic strains without failure [25-28].

To characterize the energy-absorption performance of the saw-tooth-like BMG structures, the evolution of the energy absorption per unit volume (W_v) is plotted in Fig. 2b, according to the equation [34]

$$W_v = \int_0^{\varepsilon_D} \sigma(\varepsilon)\, d\varepsilon \qquad (3)$$

where $\sigma(\varepsilon)$ is the nominal stress and ε_D the macroscopic strain. It can be seen that specimens A-C have W_v values of about 230 MJ/m^3, 270 MJ/m^3 and 320 MJ/m^3, respectively, at the onset of the densification stage. These values are much larger than the ones in the cellular BMGs with macroscopic cellular structures, which have been reported to have the best energy-absorption performance of cellular BMGs [23]. When compared at a similar relative density of about 0.5 and ε_D = 0.4, the present saw-tooth-like BMG structure shows enhanced energy absorption capacity (about 178 MJ/m^3 for specimen A) of about 200% (W_v = 58 MJ/m^3 for the cellular BMG with ρ_r = 0.49). Further examination of the evolution of the W_v values during the plastic-flow plateau stages shows that the saw-tooth-like BMG structures have larger rates of increase as compared with the cellular BMGs. This phenomenon can be attributed to the increase of nominal stresses of the saw-tooth-like BMG structures during the plastic-flow plateau stages, while the cellular BMGs exist a decay in the peak stress till densification [24].

Figure 3a summarizes the energy-absorption performance of the present

saw-tooth-like BMG structures, cellular BMGs with macroscopic cellular structures [23,24], BMG foams/honeycombs [18,20,22,35] and some representative metal foams: Al and Al alloy foams [20,36,37], copper foams [11], steel foams [38,39], Zn alloy foams [40], and composite metal foams [12,13,41,42]. It is found that the fabricated saw-tooth-like BMG structures have substantially enhanced energy absorption capacity as compared with the existing cellular solids, including metal foams and cellular BMGs. The enhancement of the energy-absorption performance of the saw-tooth-like BMG structures, as compared with the conventional metal foams, can be understood to be due to two factors: the relatively-higher strength of the parent materials [21] and the deformation behavior of the macroscopic cellular structures [24]. However, when compared with the existing BMG structures, since the strength of the parent BMGs ($Zr_{57}Cu_{20}Al_{10}Ni_8Ti_5$ BMG) of the saw-tooth-like BMG structures is not higher than the value of the reported BMG structures [23], the enhancement of the energy-absorption performance appears to mainly result from the deformation behavior of the designed saw-tooth-like structures.

After densification, one typical tooth unit of the saw-tooth-like BMG structures is given in Fig. 3(b-e). Differing from previously reported cellular BMGs, in which the deformation modes are mainly bending, buckling and collapse of structural units [17,18,21,43], the deformation mode of the tooth unit in the present saw-tooth-like BMG structures is primarily plastic deformation through shear-banding. The SEM images (Figs. 3c-e) show that, during the compressive testing process, the tooth unit

has undergone large plastic deformation, which is evidenced by the observation of a large number of shear bands. The top part of the tooth unit (Fig. 3c) has shear band patterns with three shear-banding directions, indicating the occurrence of many shear-band intersections. The bottom part of the tooth unit (Fig. 3d) also has dense shear-band patterns with two shear-banding directions as well as intersections. The dense shear-band patterns as well as the shear-band intersections on the tooth unit validate the accommodation of a huge amount of mechanical energy during the compression tests [44,45]. The formation of the shear-band patterns can be understood from effect of the gradient distribution of the stresses. Under compressive loading, the trapezoidal geometry of the tooth unit creates a gradient distribution of the stresses, where the top part has the strongest stress concentrations to initiate more shear bands than the bottom part, agreeing well with previous findings under complex stress states [25,26,29,30]. On the other hand, besides the observation of dense shear-band patterns on the surface of the tooth unit, two major shear processes without fracture (as indicated by the red arrows in Fig. 3b) are also observed. It can be speculated that, during each major shearing process, the top part of the tooth unit was compressed to slide down without fracture, resulting in large macroscopic strains to accommodate the mechanical energy. It can be summarized that the formation of the dense shear-band patterns and the shearing processes without fracture play key roles in achieving the excellent energy-absorption performance in the saw-tooth-like BMG structures. Moreover, at the region between the tooth unit and the substrate, a series of shear bands can also be observed (Fig. 3e), which are roughly perpendicular to the

loading direction. This suggests that, if the compressive loading process proceeds, the plastic deformation may extend to the substrate to accommodate more mechanical energy. Actually, this predication has been verified by the observation of a large number of shear bands on the substrate in the specimens with 52.8% nominal strain (Fig. 4b).

Besides the excellent energy-absorption performance, another advantage of saw-tooth-like BMG structures is their designable potential. Since the saw-tooth-like BMG structure consists of periodically distributed tooth units, if we ignore the effect caused by the neighboring tooth unit, the overall energy-absorption performance should be proportional to the number of tooth units, leading to the relationship

$$W_{\mathrm{v}} = n\bar{w}_{\mathrm{v}} \qquad (4)$$

where n is the number of tooth unit and $\bar{w}_{\mathrm{v}}$ is the average energy absorption capacity of each tooth unit. Based on the experimental values of specimens A-C, $\bar{w}_{\mathrm{v}}$ was estimated using the equation

$$\bar{w}_{\mathrm{v}} = \frac{1}{3}\left(\frac{W_{\mathrm{v-A}}}{n_{\mathrm{A}}} + \frac{W_{\mathrm{v-B}}}{n_{\mathrm{B}}} + \frac{W_{\mathrm{v-C}}}{n_{\mathrm{C}}}\right) \qquad (5)$$

where $W_{\mathrm{v\text{-}A}}$, $W_{\mathrm{v\text{-}B}}$ and $W_{\mathrm{v\text{-}C}}$ are the energy absorption capacities of specimens A-C, respectively, and n_{A}, n_{B} and n_{C} are the corresponding number of tooth units. Taking the value at the onset of the densification stage as the energy absorption capacity of specimens A-C, the values of $W_{\mathrm{v\text{-}A}}$, $W_{\mathrm{v\text{-}B}}$ and $W_{\mathrm{v\text{-}C}}$ were estimated at 230 MJ/m^3, 270 MJ/m^3 and 320 MJ/m^3, respectively. The average energy absorption capacity of the

tooth unit ($\overline{w}_v$) was then calculated as 43.7 ± 3.7 MJ/m^3. Therefore, for saw-tooth-like BMG structures with tooth unit number n = 7, 4 and 3, the W_v values were estimated at 306 ± 26 MJ/m^3, 175 ± 15 MJ/m^3 and 131 ± 11 MJ/m^3, respectively. As shown in Fig. 3a, the estimated values are also much larger than those in existing cellular BMGs.

Although the energy-absorption performance of the saw-tooth-like BMG structures was mainly influenced by the deformation behavior of the tooth units, other factors relating to the relative densities, such as the distance between the neutral planes of the tooth units (d_3 in Fig. 1) and the thickness of the substrate (h_2 in Fig. 1), also affect the overall performance of the structures. On the one hand, the decrease of distance between the tooth units not only increases the relative density of the BMG structures (eq. 1), but also affects the deformation behavior of neighboring tooth units. It can be seen in Fig. 4a, the tooth unit has contacted a neighboring tooth unit, causing the decrease of the onset strain for the densification stage (Fig. 2). On the other hand, the aforementioned plastic deformation in the substrate could increase the capacity for energy-absorption. For example, the continuous compressive testing of specimen B during the densification stage has shown contact between the tooth units and the substrate (Fig. 4b). In the magnified SEM image (Figs. 4c), the contact of the top part of the tooth unit cause the formation of profuse shear bands in the substrate, similar to the indentation tests [46,47]. Furthermore, in the region below the deformed tooth unit, a large number of shear bands are also formed throughout the substrate (Fig. 4d). The

formation of a larger number of shear bands in the substrate implies that, even after densification, the saw-tooth-like BMG structures still have great potential to deform plastically and accommodate a large amount of mechanical energy. Specimen B exhibited an energy absorption capacity W_v of about 419 MJ/m^3 at a nominal strain of about 53% (the value is about 270 MJ/m^3 at the onset of the densification stage, i.e., ε_{onset} = 43%).

To obtain stable nominal-stresses during the plastic-flow plateau stages is critical for achieving better energy-absorption performance in structural materials [7,24]. In the present work, continuous increasing of the nominal stress during the plastic-flow plateau stages has been achieved in BMG structures by creating gradient distributed stresses though geometric design. The findings suggest that, although BMGs have a work-softening nature and overall brittleness [48,49], the work-hardening-like behavior of BMGs under complex stress states [25] can still be employed to enhance the energy-absorption performance of BMG structures. In practical structural materials, the struts always deform under complex stress states but seldom under uniformly distributed stress states [29,31]. Therefore, the use of the deformation behavior of BMGs under complex stress states in designing BMG structures could have large potential for widespread applications in industry. The saw-tooth-like structures made of a high-strength stainless steel demonstrated W_v values of about 122 MJ/m^3, 145 MJ/m^3 and 180 MJ/m^3 at the onset of the densification stages (Fig. 3a), which are also much larger than the composite metal foams [12,13,41,42] and steel

foams [38,39]. This indicates that the using of other BMGs or alloys with higher strengths may further improve the energy-absorption performance. Additionally, as compared with microscopic cellular structures in metal foams [50,51], the controllable geometry enables the corresponding properties to become designable. Besides the periodic distribution of the tooth units, the tooth geometry and the substrate thickness could also be changed, providing a feasible route to optimize the energy-absorption properties for practical applications.

4. Conclusions

In summary, some saw-tooth-like BMG structures have been fabricated, and exhibited greatly enhanced energy absorption capacity than previously reported metal foams and BMG structures. Under compressive testing, the resultant stress gradient results in large plastic deformation in the structural units, leading to wide plastic-flow plateau stages with continuous increasing of the nominal stresses. The change of the mechanical energy accommodation route, from bending, buckling and collapse of struts in cellular metals to large plastic deformation in the present saw-tooth-like BMG structures, is responsible for the improvement of the energy-absorption performance. Moreover, the tunable distributions of the structural units, as well as geometric changes, can provide a feasible route to obtain BMG structures with desired properties.

Acknowledgements

The work described in the paper was supported by the Research Committee of The Hong Kong Polytechnic University under the project code G-YBE1.

References

[1] F.S. Han, Z.G. Zhu, J.C. Gao, Compressive deformation and energy absorbing characteristic of foamed aluminum, Metall. Mater. Trans. A, 29 (1998) 2497-2502.

[2] A.G. Evans, J.W. Hutchinson, M.F. Ashby, Cellular metals, Curr. Opin. Solid. St. M., 3 (1998) 288-303.

[3] L.J. Gibson, Mechanical behavior of metallic foams, Annu. Rev. Mater. Sci., 30 (2000) 191-227.

[4] J. Banhart, Manufacture, characterisation and application of cellular metals and metal foams, Prog. Mater. Sci., 46 (2001) 559-U553.

[5] X. Tang, V. Prakash, J.J. Lewandowski, G.W. Koolstra, H.N.G. Wadley, Inertial stabilization of buckling at high rates of loading and low test temperatures: Implications for dynamic crush resistance of aluminum-alloy-based sandwich plates with lattice core, Acta Mater., 55 (2007) 2829-2840.

[6] L. Salari-Sharif, T.A. Schaedler, L. Valdevit, Energy dissipation mechanisms in hollow metallic microlattices, J. Mater. Res., 29 (2014) 1755-1770.

[7] A.G. Evans, J.W. Hutchinson, M.F. Ashby, Multifunctionality of cellular metal systems, Prog. Mater. Sci., 43 (1998) 171-221.

[8] A. Wiest, C.A. MacDougall, R.D. Conner, Optimization of cellular solids for energy absorption, Scripta Mater., 84-85 (2014) 7-10.

[9] K.Y.G. McCullough, N.A. Fleck, M.F. Ashby, Uniaxial stress-strain behaviour of aluminium alloy foams, Acta Mater., 47 (1999) 2323-2330.

[10] C. Park, S.R. Nutt, PM synthesis and properties of steel foams, Mater. Sci. Eng.

A, 288 (2000) 111-118.

[11] S.K. Hyun, H. Nakajima, Anisotropic compressive properties of porous copper produced by unidirectional solidification, Mater. Sci. Eng. A, 340 (2003) 258-264.

[12] L.J. Vendra, A. Rabiei, A study on aluminum-steel composite metal foam processed by casting, Mater. Sci. Eng. A, 465 (2007) 59-67.

[13] A. Rabiei, L.J. Vendra, A comparison of composite metal foam's properties and other comparable metal foams, Mater. Lett., 63 (2009) 533-536.

[14] M.F. Ashby, A.L. Greer, Metallic glasses as structural materials, Scripta Mater., 54 (2006) 321-326.

[15] A. Inoue, F.L. Kong, S.L. Zhu, E. Shalaan, F.M. Al-Marzouki, Production methods and properties of engineering glassy alloys and composites, Intermetallics, 58 (2015) 20-30.

[16] J. Plummer, W.L. Johnson, Is metallic glass poised to come of age?, Nat. Mater., 14 (2015) 553-555.

[17] A.H. Brothers, D.C. Dunand, Ductile bulk metallic glass foams, Adv. Mater., 17 (2005) 484-486.

[18] A.H. Brothers, D.C. Dunand, Plasticity and damage in cellular amorphous metals, Acta Mater., 53 (2005) 4427-4440.

[19] M.D. Demetriou, C. Veazey, J.S. Harmon, J.P. Schramm, W.L. Johnson, Stochastic metallic-glass cellular structures exhibiting benchmark strength, Phys. Rev. Lett., 101 (2008) 145702.

[20] X. Wei, J.H. Chen, L.H. Dai, Energy absorption mechanism of open-cell

Zr-based bulk metallic glass foam, Scripta Mater., 66 (2012) 721-724.

[21] B. Sarac, J. Ketkaew, D.O. Popnoe, J. Schroers, Honeycomb Structures of Bulk Metallic Glasses, Adv. Funct. Mater., 22 (2012) 3161-3169.

[22] B. Sarac, J. Schroers, From brittle to ductile: Density optimization for Zr-BMG cellular structures, Scripta Mater., 68 (2013) 921-924.

[23] S.H. Chen, K.C. Chan, F.F. Wu, L. Xia, Pronounced energy absorption capacity of cellular bulk metallic glasses, Appl. Phys. Lett., 104 (2014) 111907.

[24] S.H. Chen, K.C. Chan, F.F. Wu, L. Xia, Achieving high energy absorption capacity in cellular bulk metallic glasses, Sci. Rep., 5 (2015) 10302.

[25] L.Y. Chen, Q. Ge, S. Qu, Q.K. Jiang, X.P. Nie, J.Z. Jiang, Achieving large macroscopic compressive plastic deformation and work-hardening-like behavior in a monolithic bulk metallic glass by tailoring stress distribution, Appl. Phys. Lett., 92 (2008) 211905.

[26] W.F. Wu, C.Y. Zhang, Y.W. Zhang, K.Y. Zeng, Y. Li, Stress gradient enhanced plasticity in a monolithic bulk metallic glass, Intermetallics, 16 (2008) 1190-1198.

[27] S.H. Chen, K.C. Chan, L. Xia, Effect of stress gradient on the deformation behavior of a bulk metallic glass under uniaxial tension, Mater. Sci. Eng. A, 574 (2013) 262-265.

[28] S.H. Chen, K.C. Chan, L. Xia, Fracture Morphologies of Zr-Based Bulk Metallic Glasses Under Different Stress States, Adv. Eng. Mater., 17 (2015) 366-373.

[29] S.H. Chen, K.C. Chan, L. Xia, Deformation behavior of bulk metallic glass structural elements, Mater. Sci. Eng. A, 606 (2014) 196-204.

[30] S.H. Chen, K.C. Chan, L. Xia, Deformation behavior of a Zr-based bulk metallic glass under a complex stress state, Intermetallics, 43 (2013) 38-44.

[31] G. Kumar, A. Desai, J. Schroers, Bulk Metallic Glass: The Smaller the Better, Adv. Mater., 23 (2011) 461-476.

[32] Y.J. Huang, J. Shen, J.F. Sun, Bulk metallic glasses: Smaller is softer, Appl. Phys. Lett., 90 (2007) 081919.

[33] F.F. Wu, Z.F. Zhang, S.X. Mao, J. Eckert, Effect of sample size on ductility of metallic glass, Phil. Mag. Lett., 89 (2009) 178-184.

[34] L.J. Gibson, M.F. Ashby, Cellular Solids Structure and Properties, Cambridge University Press, Cambridge, 1997.

[35] T. Wada, A. Inoue, Formation of porous Pd-based bulk glassy alloys by a high hydrogen pressure melting-water quenching method and their mechanical properties, Mater. Trans., 45 (2004) 2761-2765.

[36] F. Yi, Z.G. Zhu, F.Q. Zu, S.S. Hu, P. Yi, Strain rate effects on the compressive property and the energy-absorbing capacity of aluminum alloy foams, Mater. Charact., 47 (2001) 417-422.

[37] A.E. Markaki, T.W. Clyne, The effect of cell wall microstructure on the deformation and fracture of aluminium-based foams, Acta Mater., 49 (2001) 1677-1686.

[38] O. Andersen, U. Waag, L. Schneider, G. Stephani, B. Kieback, Novel metallic hollow sphere structures, Adv. Eng. Mater., 2 (2000) 192-195.

[39] B.P. Neville, A. Rabiei, Composite metal foams processed through powder

metallurgy, Mater. Design., 29 (2008) 388-396.

[40] S.R. Yu, J.A. Liu, M. Wei, Y.R. Luo, X.Y. Zhu, Y.H. Liu, Compressive property and energy absorption characteristic of open-cell ZA22 foams, Mater. Design., 30 (2009) 87-90.

[41] G.H. Wu, Z.Y. Dou, D.L. Sun, L.T. Jiang, B.S. Ding, B.F. He, Compression behaviors of cenosphere-pure aluminum syntactic foams, Scripta Mater., 56 (2007) 221-224.

[42] A. Daoud, M.T. Abou El-Khair, M. Abdel-Aziz, P. Rohatgi, Fabrication, microstructure and compressive behavior of ZC63 Mg-microballoon foam composites, Compos. Sci. Technol., 67 (2007) 1842-1853.

[43] M.D. Demetriou, J.C. Hanan, C. Veazey, M. Di Michiel, N. Lenoir, E. Ustundag, W.L. Johnson, Yielding of metallic glass foam by percolation of an elastic buckling instability, Adv. Mater., 19 (2007) 1957-1962.

[44] S.X. Song, T.G. Nieh, Flow serration and shear-band viscosity during inhomogeneous deformation of a Zr-based bulk metallic glass, Intermetallics, 17 (2009) 762-767.

[45] B.A. Sun, W.H. Wang, Fractal nature of multiple shear bands in severely deformed metallic glass, Appl. Phys. Lett., 98 (2011) 201902.

[46] S. Jana, U. Ramamurty, K. Chattopadhyay, Y. Kawamura, Subsurface deformation during Vickers indentation of bulk metallic glasses, Mater. Sci. Eng. A, 375 (2004) 1191-1195.

[47] Y.F. Gao, L. Wang, H. Bei, T.G. Nieh, On the shear-band direction in metallic

glasses, Acta Mater., 59 (2011) 4159-4167.

[48] A.R. Yavari, J.J. Lewandowski, J. Eckert, Mechanical properties of bulk metallic glasses, MRS Bull., 32 (2007) 635-638.

[49] M.M. Trexler, N.N. Thadhani, Mechanical properties of bulk metallic glasses, Prog. Mater. Sci., 55 (2010) 759-839.

[50] A.E. Simone, L.J. Gibson, Effects of solid distribution on the stiffness and strength of metallic foams, Acta Mater., 46 (1998) 2139-2150.

[51] A.H. Brothers, D.C. Dunand, Amorphous metal foams, Scripta Mater., 54 (2006) 513-520.

Figure captions

Figure 1. (a) The schematic diagram of the designed saw-tooth-like BMG structures, where h_1 = 2 mm, h_2 = 1 mm, w = 2 mm, d_1 = 0.33 mm, d_2 = 1 mm, and d_3 = 2.8 mm, 2.2 mm and 1.6 mm respectively for specimens A, B and C, respectively. (b) The schematic diagram showing the compressive testing of the saw-tooth-like structures.

Figure 2. The compressive testing results of the saw-tooth-like BMG structures (a) and the corresponding evolution of the energy absorption capacity (W_v) of the saw-tooth-like BMG structures (b). The dash lines in (b) show the evolution of W_v of two cellular BMGs with macroscopic cellular structures [23] for comparison.

Figure 3. (a) Comparison of the energy absorption capacity per unit volume (W_v) of the saw-tooth-like BMG structures with other cellular solids: (1) saw-tooth-like BMG structures in the present work; (2) Estimated values in saw-tooth-like BMG structures with other relative densities; (3) Saw-tooth-like structures made of a high-strength stainless steel; (4) Cellular BMGs with macroscopic cellular structures [23,24]; (5) BMG foams [18,20,35] and honeycombs [22]; (6) Composite metal foams [12,13,41,42]; (7) Cu foams [11]; (8) Steel foams [38,39]; (9) Zn-22Al alloy foams [40] and (10) Al and Al alloy foams [20,36,37]. (b-c) SEM images of one typical tooth unit in specimen A after densification, where (c-e) are magnified images of the rectangles F, G and H in (b) respectively. The red arrows in (b) indicate the major

sliding processes in the tooth unit, and the dashed lines in (c-e) show the shear-banding directions.

Figure 4. (a) and (b) are SEM images showing the typical tooth units of specimens C and B, respectively, after densification. (c) and (d) are the magnified SEM images of rectangles M and N in (b), respectively.

Graphical Abstract (for review)

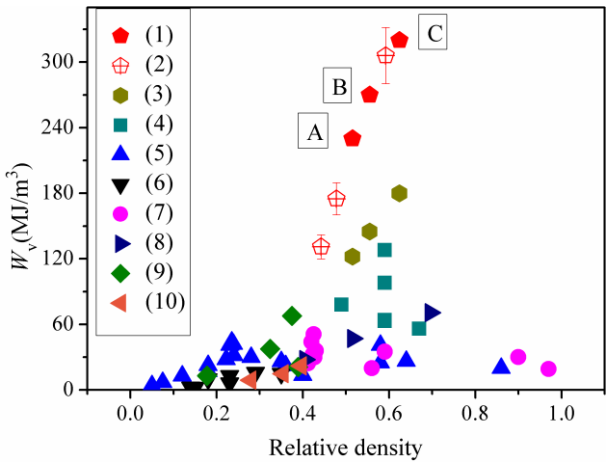

S. H. Chen *et al*.

Graphical abstract

Figure1

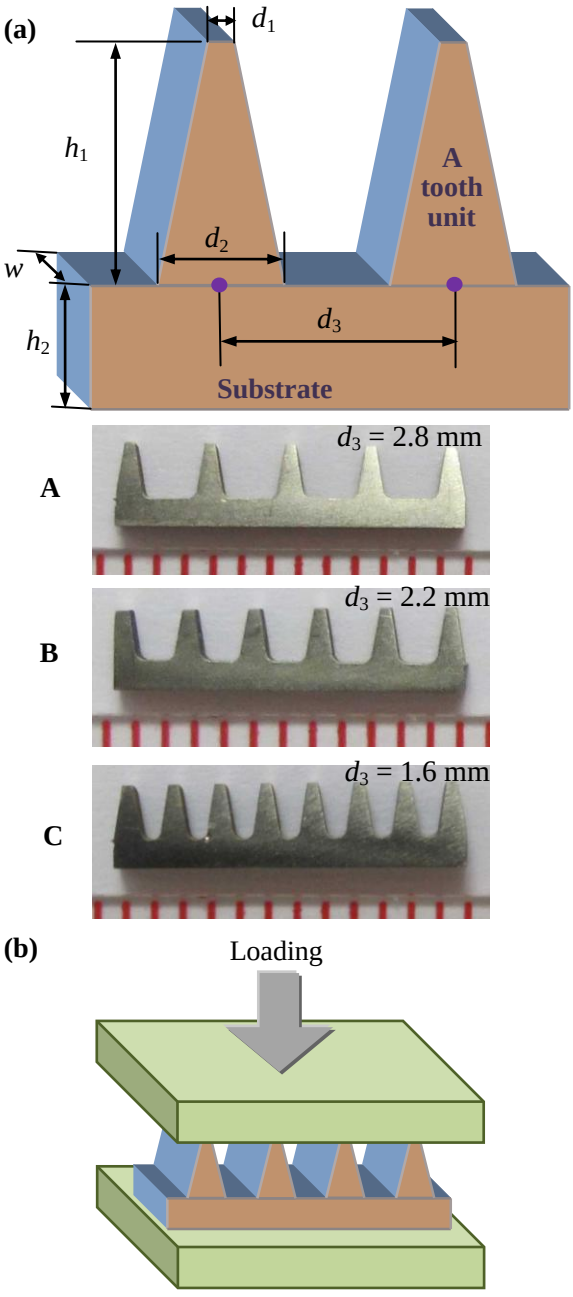

S. H. Chen *et al.*

Figure 1

Figure 2

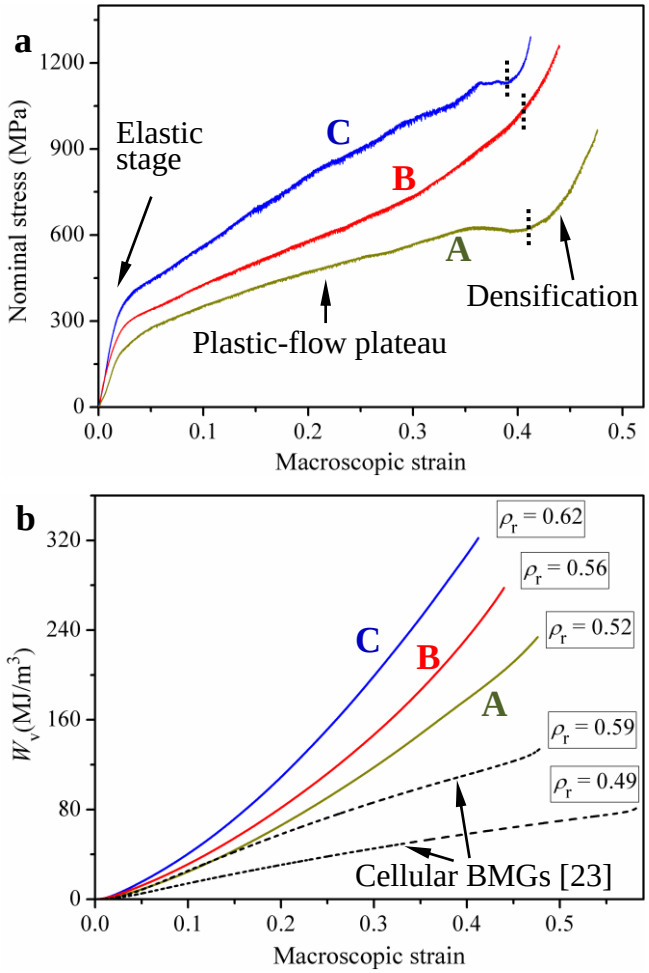

S. H. Chen *et al.*

Figure 2

Figure3

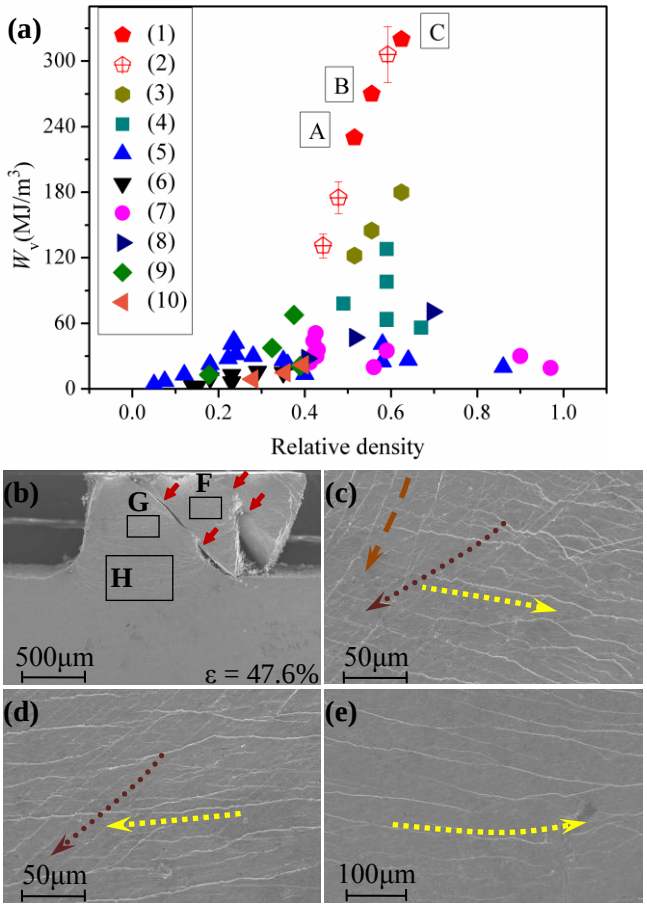

S. H. Chen *et al.*

Figure 3

Figure 4

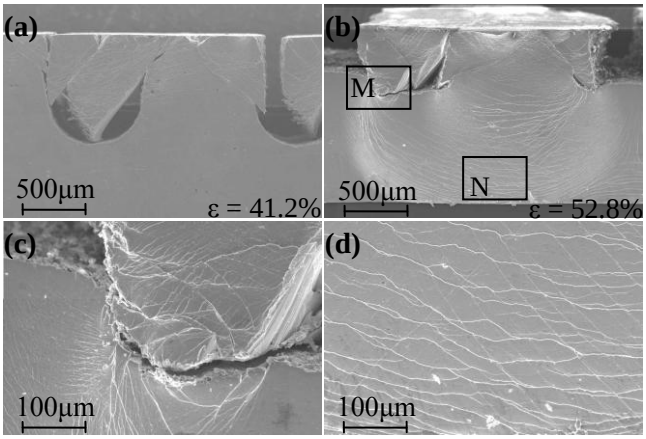

S. H. Chen *et al*.

Figure 4